

## Physical Mechanisms of High-Enthalpy Initiation

A. P. Ershov<sup>a</sup>, A. O. Kashkarov<sup>a</sup>, and E. R. Prueel<sup>a</sup>

UDC 662.215.1

Published in *Fizika Goreniya i Vzryva*, Vol. 51, No. 6, pp. 85–95, November–December, 2015.  
Original article submitted September 3, 2014.

**Abstract:** Injection of a hot gas flow produced by an external source into a powdered explosive allows very fast (within a few microseconds) deflagration-to-detonation transition. Under this high-enthalpy initiation conditions, the process begins with the stage of convective combustion, and the initial velocity of the wave is about 1 km/s. The combustion kinetics known from the literature does not provide the observed rapid development of the process. Various mechanisms of acceleration of the reaction are considered. Results of calculation for a two-phase gas-dynamic model are compared with data of synchrotron diagnostics (set of density profiles in the wave).

**Keywords:** detonation, initiation, convective combustion, deflagration-to-detonation transition, two-phase media.

**DOI:** 10.1134/S0010508215060118

### INTRODUCTION

Historically, the initiation of a number of explosives in a time of about 10  $\mu$ s has been observed in studies of detonation transfer through an air gap. According to [1, 2], in the case of powdered explosive, detonation is initiated by ignition of explosive grains by the hot gas flow generated by the explosion of an active charge, with the combustion rapidly propagating due to the pressure of the flow impinging on the charge.

Later, similar processes have been studied in connection with the development of safe systems of initiation of secondary explosives. A review of these studies is presented in [3]. The development of normal detonation in about 10  $\mu$ s was implemented by powerful electrical explosion of a wire placed in an explosive powder. The same results have been obtained by initiating explosive powders by flow of powder combustion products from a separate chamber after rupture of a calibrated membrane or by flow of gaseous detonation products. In all these cases, as in [1, 2], hot gas flow is introduced into the porous bed of a loose-packed charge. With sufficient intensity, this high-enthalpy flow causes vigorous convective burning of the explosive, which proceeds

to detonation. In contrast to the standard scenario of deflagration-to-detonation transition occurring after ignition at low pressure [4], the initial slow stage of layer-by-layer combustion is excluded. Therefore, the process develops so fast that successful transition to detonation is possible even without a strong shell. As a result, it is possible to carry out the transition within the diameter of a standard detonator, which is used in practice [3].

The initial dynamic pressure of the initiating flow (several hundred atmospheres) is significantly lower than that required to ignite a powder by a shock wave (see, e.g., [5]). Studies of the flow structure [6, 7] have confirmed that in the initial stage of initiation, a shock wave is not observed in the material. A compression wave with a smooth front propagates in the powder at a velocity of about 1 km/s; the compaction of the material is insignificant ( $\approx 20\%$ ) and insufficient for pore closure. The process is substantially two-phase and is driven by the high-temperature gas flow filtration through the pores due to the pressure difference at the wave front.

At the relatively low pressures occurring at the initial stage of initiation, the burning rate of the explosive is also small. Elementary estimates and numerical calculations [8] have shown that the standard rate of surface regression [9] is about an order of magnitude less than that required to sustain and then accelerate the two-phase flow. Thus, there is the problem of a theo-

<sup>a</sup>Lavrent'ev Institute of Hydrodynamics, Siberian Branch, Russian Academy of Sciences, Novosibirsk, 630090 Russia; ers@hydro.nsc.ru.

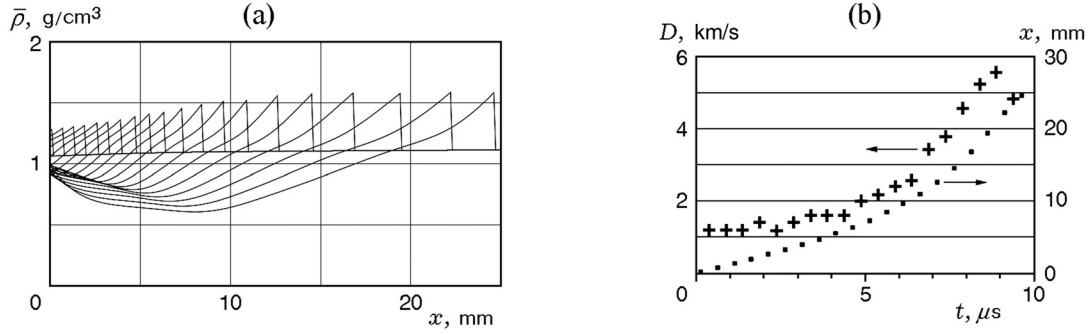


**Fig. 1.** Near-limit initiation regime (time of the process 9.5  $\mu\text{s}$ ); the density distribution along the axis of the charge (step of 0.5  $\mu\text{s}$ ) (a) and the kinematics of the wave front (b).

retical description of the process which should include the mechanism (or mechanisms) of combustion intensification. A numerical model that allows calculated flow fields to be compared with data of synchrotron diagnostics of the process is described in [8]. It has been shown that consideration of some effects of acceleration of the reaction brings closer the results of calculations and experiments. However, the obtained agreement was rather qualitative. In the present paper, a wider range of possible mechanisms of reaction acceleration is considered, which makes it possible to select the most appropriate of them and obtain the best agreement with experimental data.

## 1. FORMULATION OF THE PROBLEM

The experimental setup is described in detail in [8]. A loose-packed PETN charge 16 mm in diameter was initiated from the open end by the hot gas flow produced by explosion of another (active) charge of PETN. The test charge was irradiated by a synchrotron radiation (SR) beam from a VEPP-3 accelerator (Siberian Center of Synchrotron Radiation). The absorption of the SR is determined by the mass on its way. Processing of the detector records, a procedure similar to X-ray tomography, gives a set of density distributions in the charge with a time step of 0.5  $\mu\text{s}$  (Fig. 1a). The aim of the simulation was to reproduce these distributions. In addition, the kinematics of the compression wave front in the charge is clearly identified (see Fig. 1b), which was also used for comparison with the calculations.

The calculated configuration is shown in Fig. 2. The one-dimensional nonstationary problem was solved. The active charge for which the instantaneous detonation parameters were specified at the initial time was adjusted to provide the specified parameters of the air shock wave incident on the boundary of the investigated

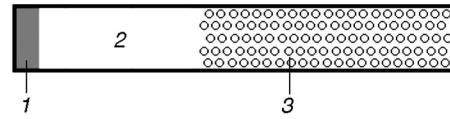


**Fig. 2.** Geometry of the computational domain: (1) active charge; (2) air gap; (3) porous charge.

charge. The focus was on the case of rather mild action (sufficient, however, for detonation development in the indicated dimensions). In this regime before the contact with the powder, the gas flow velocity is  $u = 2.2$  km/s and the incident air shock wave pressure is  $p \approx 10$  MPa, which corresponds to a pressure of 90 MPa in reflection from a rigid wall. The test charge is located in a region  $0 < x < 25$  mm.

For the numerical simulation, we used a two-phase two-velocity system of equations, basically similar to that presented in [8]:

$$\begin{aligned}
 \frac{\partial \rho \varphi}{\partial t} + \frac{\partial \rho \varphi u}{\partial x} &= J, \\
 \frac{\partial \rho \varphi u}{\partial t} + \frac{\partial \rho \varphi u^2}{\partial x} + \varphi \frac{\partial p}{\partial x} &= Jv - f, \\
 \frac{\partial \rho \varphi E_g}{\partial t} + \frac{\partial \rho \varphi u E_g}{\partial x} + p \frac{\partial (\varphi u + \alpha v)}{\partial x} \\
 &= J \left( Q + \frac{(u-v)^2}{2} + E_s \right) + f(u-v) - q, \\
 \rho_s \left( \frac{\partial \alpha}{\partial t} + \frac{\partial \alpha v}{\partial x} \right) &= -J, \\
 \frac{\partial v}{\partial t} + \frac{1}{2} \frac{\partial v^2}{\partial x} + \frac{1}{\rho_s} \frac{\partial p}{\partial x} + \frac{1}{\rho_s \alpha} \frac{\partial p_s}{\partial x} &= \frac{f}{\rho_s \alpha}, \\
 \frac{\partial E_s}{\partial t} + v \frac{\partial E_s}{\partial x} + \frac{p_s}{\rho_s \alpha} \frac{\partial v}{\partial x} &= \frac{q}{\rho_s \alpha}, \\
 p_s &= p_s(\varphi, \varphi_{\min}), \quad E_s = C(T_s - T_0) + E_p,
 \end{aligned} \tag{1}$$

$$p = p(\rho, E_g), \quad T = T(\rho, E_g).$$

Here  $t$  is time,  $x$  is the coordinate,  $\rho$  is the density of the gas,  $\rho_s$  is the constant crystal density of the explosive,  $\alpha$  is the volume fraction of the solid phase,  $\varphi$  is the porosity,  $\alpha + \varphi = 1$ ,  $u$  and  $v$  are the velocities of the gas and solid phase, respectively,  $E_g$  and  $E_s$  are the internal energies of the gas and solid phase,  $p$  is the gas pressure,  $p_s$  is the compression pressure of the solid skeleton,  $T$  and  $T_s$  are the average temperatures of the gas and the solid phase,  $C$  is the specific heat of the explosive,  $f$  is the interfacial friction force,  $q$  is the heat exchange term,  $J$  is the mass flux from the solid to the gas phase, and  $Q$  is the heat of the reaction.

The equation of state of the gas from [10] was used. For the powder, the pressure  $p_s$  was determined in the same way as in [8]. In particular, in the compression phase,

$$p_s = \rho_s c_{0s}^2 \left[ (1 - \beta)(\varphi_0 - \varphi) + \beta \varphi_0 \left( \frac{\varphi_0}{\varphi} - 1 \right) \right]. \quad (2)$$

Here  $c_{0s}$  is the velocity of sound in the powder for the initial state at  $\varphi = \varphi_0 = 0.42$  and  $\beta$  is the fitting coefficient. The parameters  $\beta = 0.25$  and  $c_{0s} = 0.22$  km/s were selected so as to provide the best fit to the experiment [11].

For heat exchange in the simplest case, the Denton correlation is used [12]:

$$\begin{aligned} q &= ASG, \\ G &= \text{Nu} \frac{\lambda(T - T_s)}{d}, \\ \text{Nu} &= 2 + 0.6 \left( \frac{\rho|u - v|d\varphi}{\eta} \right)^{0.7}. \end{aligned} \quad (3)$$

Here  $A$  is the specific surface area (per unit volume) of the powder,  $G$  is the specific heat flux per unit particle surface area,  $\lambda$  is the thermal conductivity of the gas,  $\text{Nu}$  is the Nusselt number, and  $\eta$  is the dynamic viscosity of the gas. In the initial state ( $\varphi = \varphi_0$ ),  $A = 6(1 - \varphi_0)/d$  for spherical particles of diameter  $d$ . Increase in the specific surface area due to fragmentation is taken into account by the coefficient  $S > 1$ . The factor  $S$  is also included in the friction force  $f$  (whose form is given in [8]) and the interfacial mass transfer  $J$ . The fragmentation effect is discussed in detail below.

System (1) is a two-temperature one. The reaction in the simplest case started upon reaching the predetermined average temperature of the solid phase  $T_s$ , which was selected to provide the best possible agreement with experiment. Actually, a thin layer on the particle surface is heated, in which the temperature is significantly higher (about 1000 K, if the difference  $T_s - T_0$  was varied from a few to tens of degrees [8]).

## 2. COMBUSTION MECHANISMS

The burning rate law has the form

$$J = ASu_n,$$

where  $u_n$  is the explosive surface regression rate. In the standard case for PETN, this rate is proportional to the pressure:

$$u_n = Bp \quad (4)$$

( $u = 11$  cm/s at  $p = 100$  MPa [9]). The main problem in the modeling, as already mentioned, is the low standard burning rate of the explosive. In the calculation [8], a slowly moving ( $\approx 400$  m/s), almost impenetrable plug of compacted explosive is formed, and ignition occurs at the rear end of the plug. The released energy is insufficient to sustain the wave, so that the process slowly decays. In the real situation, the slow dynamics of the process would lead to failure due to side expansion.

Estimates show that there may be three mechanisms capable of increasing the overall reaction rate by an order of magnitude in the initial stage of initiation.

(1) Fragmentation of the explosive particles due to both powder compaction and the aerodynamic pressure from the flow filtration through the pores. Unlike the mechanisms below, the effect is achieved due to the growth of the surface, without acceleration of the reaction on the interface.

(2) Acceleration of the explosive burning due to the heat flow from the gas phase, which can significantly exceed the flow under conventional combustion conditions. In rocket motors, this effect is called erosive burning.

(3) Shear instability of the evaporating explosive grain boundary, resulting in the separation and rapid combustion of microscopic gas volumes. This mechanism, at the suggestion of L. A. Luk'yanchikov, will be called the ablative one.

Fragmentation processes in the cases of compaction, ablation, and their joint action are considered in [8]. The last case turned out to be the closest to the experiment. In this paper, we study a wider range of processes that can accelerate the reaction.

### 2.1. Particle Fragmentation

In [8], only fragmentation due to compaction was considered, i.e., the surface increase coefficient  $S$  was determined by the minimum porosity of the powder  $\varphi^*$  reached at a given Lagrangian point. The dependence  $S(\varphi^*)$  approximated the data [4]:

$$S = 1 + 4 \left( \frac{1}{\varphi^*} - \frac{1}{\varphi_0} \right). \quad (5)$$

We can equally well use the dependence of  $S$  on the maximum solid pressure  $p_s^*$  in the given particle by expressing  $\varphi(p_s)$  from (2):

$$\varphi = \varphi_0 - \frac{\varphi_0 + P - \sqrt{(\varphi_0 + P)^2 - 4\varphi_0 P(1 - \beta)}}{2(1 - \beta)}, \quad (6)$$

$$P = \frac{p_s}{\rho_s c_{0s}^2}.$$

The dependence  $S(p_s^*)$  which follows from (5), (6) can be briefly written as

$$S = F(p_s^*). \quad (7)$$

This made it possible to obtain sufficiently rapid initiation, but the shock-wave dynamics differed sharply from the experimental one. In particular, at the beginning of the process, the compression wave velocity in the powder is low due to the inertia of the solid phase accelerated by the low-density gas flow. A narrow peak of compaction of the solid phase form, which serves as the ignition site, is formed only in a few microseconds. In contrast, in the experiment, the density in the wave increases monotonically and smoothly (see Fig. 1a).

This drawback can be overcome by taking into account the aerodynamic fragmentation of the explosive particles. Gas flow filtration through the bulk-density explosive at an initial velocity of about 1 km/s lead to significant aerodynamic forces unevenly distributed on the particle surface. This gives rise to stresses that can cause breakup of the explosive grains similar to the destruction of meteorites in the atmosphere. This effect does not require any particle displacement and can occur almost instantaneously.

According to [13], the aerodynamic stresses in the particles are proportional to  $\rho(u - v)^2$ . On the other hand, the compaction-induced breaking stresses in the grains are proportional to the solid pressure  $p_s$ . It is reasonable to combine these two effects in a simplest way by assuming that the specific surface area increase coefficient depends on the maximum value of the linear combination of the solid pressure and the aerodynamic load:

$$S = F[(p_s + \theta\rho(u - v)^2)^*]. \quad (8)$$

Here the function  $F$  is the same as in (7), and  $\theta$  is a dimensionless coefficient that depends on features of the flow in the pores. Since it is now hardly possible to reliably calculate this coefficient,  $\theta$  should be treated as a variable parameter which, for a significant aerodynamic effect, should be about 0.5.

## 2.2. Erosive Burning

Typically, in combustion simulations it is assumed that after ignition, the gas flowing from the burning surface blocks interfacial heat transfer  $q$  (see, e.g., [14, 15]). Of course, in the reaction zone, as well as in the pre-heating zone, a heat flux exists but it decreases to zero

with distance from the burning surface to the zone of combustion products. Under the assumption of an equilibrium burning rate law of the form (4), the thickness of the reaction zone is neglected, i.e., the heat flux in this zone is neglected and only the external heat transfer  $q$  is considered. However, if the velocity of the hot gas flow around the explosive grains is high, the heat flux to the particle surface can significantly exceed the normal value in the reaction zone. Then, heat exchange with the gas phase will continue after surface ignition. The reaction rate will also increase. In considering the problem of solid fuel combustion in rocket motors, this effect is called erosive burning.

Analysis of the literature has shown that existing models are hardly applicable to our two-phase system. Earlier semi-empirical approaches relate the erosive effect to an increase in the effective thermal conductivity in turbulent flow. These theories have a number of disadvantages (in particular, the well-known model [16, 17] use the boundary-layer laws on an impermeable surface, i.e., they are approximations for the case of weak blowing). In addition, combustion in these theories is described using the Zel'dovich–Frank–Kamenetskii model, in which the maximum temperature is specified by the heat of reaction, whereas in our problem of high-enthalpy initiation, the gas temperature in the pores can be several times greater. Modern approaches (including combustion and turbulence models, see, e. g., [18]) are too cumbersome for use in the two-phase gas-dynamic code. Therefore, the following compromise was adopted.

In an explosive particle, we identify a surface layer in which the temperature  $T_{ss}$  due to heat flux differs from the temperature of the bulk material. The particle is ignited upon reaching the desired surface temperature  $T_{ss} = T_b$ . At the same time, the heat flux to the solid phase is reduced due to injection of combustion products (the well-known Kutateladze–Leont'ev correlation is used [19]):

$$\frac{G}{G_0} = \left(1 - \frac{2\rho_s u_n}{b_{cr} c_{f0} \rho |u - v|}\right)^2, \quad (9)$$

where  $G_0$  is the heat flux in the absence of injection, which is given by formula of the type (3), and  $c_{f0}$  is the drag coefficient of the plane surface under reference conditions (also without injection) [20]. Heat transfer ceases when the dimensionless injection parameter  $b = 2\rho_s u_n / (c_{f0} \rho |u - v|)$  reaches a critical value  $b_{cr}$ . For the case where the surface temperature  $T_b$  is below the flow temperature  $T$  outside the boundary layer, the parameter  $b_{cr}$  is defined by the expression [21]

$$b_{cr} = \frac{1}{1 - \psi} \left( \ln \frac{1 + \sqrt{1 - \psi}}{1 - \sqrt{1 - \psi}} \right)^2, \quad \psi = \frac{T_b}{T}.$$

In the quasistationary approximation where a Michelson temperature profile occurs in the solid explosive, the burning rate is approximately proportional to the heat flux  $G_s$  on the burning surface:

$$u_n = \frac{G_s}{\rho_s C(T_b - T_0)}.$$

For large values of the heat transfer  $q$ , the difference between  $G$  and  $G_s$  can be neglected, so that with a predominance of the external heat flow, the particle surface regression rate is proportional to this flux. Conversely, with a small effect of the external flux, the regression rate is standard (proportional to the pressure), so that for the general case, we use a simple interpolation similar to [22]:

$$u_n = BP + \frac{G}{\rho_s C(T_b - T_0)}. \quad (10)$$

Although expression (10) does not contain any deep idea, it gives correct asymptotics for small and large values of  $G$ . From (9) and (10), we can obtain the heat flux in combustion, which is conveniently represented as

$$G = 2G_w G_0(1 - \varepsilon)^2 \left/ \left[ \sqrt{G_w^2 + 4G_0 G_w(1 - \varepsilon)} + G_w + 2G_0(1 - \varepsilon) \right] \right., \quad (11)$$

where  $G_w = b_{cr} C(T_b - T_0) c_{f0} \rho |u - v|/2$ ,  $\varepsilon = 2\rho_s BP / (c_{f0} \rho |u - v| b_{cr})$ . At  $\varepsilon = 1$ , the flux tends to zero, and it is certainly equal to zero at  $\varepsilon > 1$  (boundary-layer displacement takes place).

The surface temperature before ignition can be calculated by solving the heat-conduction problem for a given heat flux  $G(t)$  (which is different for different Lagrangian points). However, it should be taken into account that there are no reliable data on the ignition kinetics of the explosive for these conditions and the ignition condition at  $T_{ss} = T_b$  is approximate [23]. Therefore, the ignition temperature  $T_b$  should be treated as a fitting parameter. Under these conditions, a straightforward calculation of the particle temperature distribution would be an excess of the accuracy. In addition, the introduction of an additional coordinate would complicate the code and greatly slow its operation. In view of this, we used a simplified scheme. At constant heat flux  $G$  starting at the time  $t = 0$ , the surface temperature increases in time  $t$  by the value

$$\Delta T = \frac{2G\sqrt{t}}{\sqrt{\pi\lambda_s\rho_s C}},$$

where  $\lambda_s$  is the thermal conductivity of the solid explosive. For a power-law dependence of the flux on time ( $G \propto t^n$ ), we have

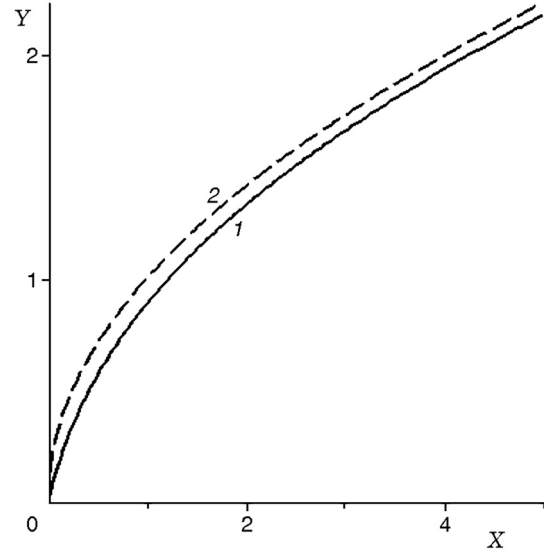


**Fig. 3.** Ignition curves: (1) universal curve from [23]; (2) dependence (13).

$$\Delta T = \frac{\Gamma(n+1)}{\Gamma(n+3/2)} \frac{G\sqrt{t}}{\sqrt{\lambda_s\rho_s C}},$$

i.e., differs in the numerical coefficient. The latter dependence was generalized in [23]. The dimensionless variables were introduced:

$$X = \frac{tG(t)}{\int_0^t G dt}, \quad Y = \sqrt{\frac{t}{\lambda_s\rho_s C}} \frac{G}{\Delta T}.$$

For the power-law dependence  $G \propto t^n$ , obviously,  $Y = \Gamma(n+3/2)/\Gamma(n+1)$  and  $X = n+1$ . This leads to the hypothesis that in a more general case,  $Y(X)$  can also be expressed as

$$Y = \frac{\Gamma(X+1/2)}{\Gamma(X)}. \quad (12)$$

For the power law  $G \propto t^n$ , this expression is exact. It has been shown [23] that for a wide range of dependences  $G(t)$ , including nonmonotonic ones, the universal curve (12) provides a good description of ignition. In fact, this coincidence implies a weak dependence of the ignition temperature on the heating conditions and a sharp transition from the inert phase of heating to the onset of the reaction.

A disadvantage of the dependence (12) is the inclusion of an explicitly fixed heating time and its reference point. In the nonstationary one-dimensional problem solved by the shock-capturing method, there may be a smooth increase of  $G$  and the time of switching-on of the heat flux at each point in space is not identified.

Analysis shows that dependence (12) can be replaced by similar dependence

$$Y = \sqrt{X}. \quad (13)$$

A comparison of these curves is shown in Fig. 3. For example, near  $X = 1$  (or  $n = 0$ ), the values of  $Y$  for curves (12) and (13) differ by approximately 10%. Note that dependence (12) holds for  $X > 1/2$  (in the case of a power dependence  $n > -1/2$ ), so that the neighborhood of  $X = 0$  [where the difference between (12) and (13) is significant] is not important. From (13), the surface temperature can be expressed as

$$T_{ss} = T_s + \sqrt{\frac{1}{\lambda_s \rho_s C}} \sqrt{G(t) \int_0^t G(t) dt}. \quad (14)$$

In contrast to (12), expression (14) does not require knowledge of the moment of switching-on of the flux, i.e., the lower limit of integration in it can mean, for example, the global start of the computation. At each point, only the values at the given time are used: the heat flux and the integral of it accumulated in the past.

Of course, formula (14) does not always apply. For example, in the case of pulsed heating, it yields zero after the lapse of the pulse time, whereas, actually, the surface temperature will decrease in proportion to the square root of time. However, we are interested in regimes with increasing temperature, for which this formula can be assumed to be valid.

From (11) and (10), the regression rate is expressed in terms of the flow parameters. For  $T_b - T_0 \simeq 10^3$  K and  $G \simeq 3 \cdot 10^{-3}$  J/(mm<sup>2</sup> · μs),  $u_n$  increases to  $\simeq 1$  m/s.

The introduction of the third (surface) particle temperature  $T_{ss}$  requires some complication of system (1). In this case, the phase energy equations were modified as follows:

$$\begin{aligned} & \frac{\partial \rho \varphi E_g}{\partial t} + \frac{\partial \rho \varphi u E_g}{\partial x} + P \frac{\partial (\varphi u + \alpha v)}{\partial x} \\ & = J \left[ Q + E_s + \Delta E_s + \frac{(u-v)^2}{2} \right] + f(u-v) - q, \\ & \frac{\partial E_s}{\partial t} + v \frac{\partial E_s}{\partial x} + \frac{P_s}{\rho_s \alpha} \frac{\partial v}{\partial x} = -\frac{J}{\rho_s \alpha} \Delta E_s + \frac{q}{\rho_s \alpha}, \end{aligned}$$

where  $\Delta E_s = T_{ss} - T_s$  is the addition to the internal energy of the surface layer of the solid phase due to heating.

### 2.3. Ablation

High-velocity flow around explosive grains leads to intense heat transfer, resulting in evaporation of the surface. The evaporating layer is subject to shear instability, which leads to its rapid separation and burnout.

Cyclic repetition of this process can provide a high temperature gradient and thus a high regression rate. This model proposed in [7], provides an acceleration of the reaction by about an order of magnitude at the initial stage of initiation.

The burning rate can be represented as

$$u_n = \frac{k}{\rho_s} \left( \frac{\lambda}{C_g d} \right)^{1/3} (\rho |u - v|)^{2/3}, \quad (15)$$

where  $C_g$  is the specific heat of the gas and  $k$  is a coefficient of order 1. At a flow velocity  $u - v = 1$  km/s, and a gas density  $\rho = 0.1$  g/cm<sup>3</sup>, the surface regression rate is about 1 m/s.

## 3. SIMULATION RESULTS

The above-mentioned mechanisms of reaction acceleration look quite reasonable. However, the applicability of the formulas is unclear. For example, the erosive mechanism suggests that combustion occurs in a developed turbulent boundary layer formed on a smooth surface. In contrast, if ablation in the above sense is significant, combustion occurs near the particle surface, which is not smooth due to instability of the process. It is not clear beforehand what alternative should be preferred. Therefore, the probable mechanisms were selected by comparing the calculated results with experimental data. Although in the initial state, all these mechanisms can provide the required acceleration of the reaction, they lead to different dynamics of the process.

### 3.1. Aerodynamic Fragmentation

As mentioned above, fragmentation due to powder compaction does not describe the experimental data. It is natural to expect that the inclusion of aerodynamic forces improves the agreement with the experiment. In the calculations, we used the burning rate law (4) and dependence (8) for the increase in the specific surface area. The ignition temperature  $T_b$  and the coefficient  $\theta$  specifying the contribution of aerodynamics were varied. The process is accelerated with increasing  $\theta$ , and by varying  $\theta$  for a given value of  $T_b$ , it is possible to achieve an integral coincidence of the kinematics, i.e., a given displacement of the shock front in the time corresponding to the end of the calculation (9.5 μs). The suitability of the mechanism considered was evaluated from the deviation of the calculated diagram  $x(t)$  from the experimental one and by comparison of the calculated density profiles with the experimental set (see Fig. 1). The values of the selected parameters should be in physically reasonable ranges (e.g.,  $T_b - T_0$  in the two-temperature

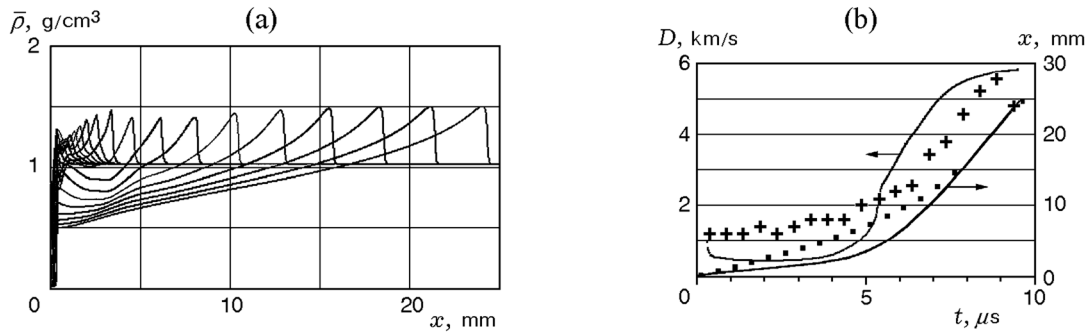


**Fig. 4.** Calculation of the near-limit regime shown in Fig. 1 taking into account aerodynamic fragmentation ( $T_b = T_0 + 5$  K and  $\theta = 0.35$ ): (a) calculated density distribution along the charge axis (step  $0.5 \mu\text{s}$ ); (b) kinematics of the wave front; points are experimental data, and curves are calculated results.

model can be of the order of 10 K and  $\theta$  cannot differ sharply from 0.5). The calculation results for the most suitable combination of these parameters are shown in Fig. 4. The value of  $\theta$  for which the kinematic agreement is achieved decreases with increasing  $T_b$ . For example, for  $T_b = T_0 + 20$ , the fitting value is  $\theta = 0.15$ .

Accounting for aerodynamic fragmentation somewhat improved the agreement with the experiment compared with the case of pure compaction [8]. Aerodynamic mechanism starts fragmentation immediately after injection of the gas flow into the pores. Growth in the specific surface area increases the heat exchange and leads to earlier ignition, resulting in a decrease in the compressibility of the medium and an increase in the velocity of the front. However, there remain substantial differences. Due to the aerodynamic effect, the interfacial friction increases and the solid phase is accelerated faster. As a result, the density in the front starts to increase sharply, which is manifested in Fig. 4a as the peak at  $x \approx 1$  mm. Next, the initiating flow is decelerated and the fragmentation effect weakens until the wave starts to develop due to the release of energy behind the front. During the first  $5 \mu\text{s}$ , the calculated wave front moves about three times slower than in the experiment, and later its sharp acceleration begins. In the density profiles at this time, a local compression maximum (at  $x \approx 3.5$  mm) is observed, although it is weaker than that in the absence of the aerodynamic effect (see Fig. 8a in [8]). In the experiment (see Fig. 1), the density at the front increases monotonically and the acceleration of the wave is smoother.

### 3.2. Erosion and Fragmentation

In the case of erosive burning, we used the three-temperature model described above and dependences (10) and (11). The surface ignition temperature  $T_b$  was varied (in the neighborhood of 1000 K).

The simulation showed that the erosion mechanism by itself does not provide the necessary dynamics of the wave. A narrow (1–2 mm) zone of rapid reaction occurred, which moved at a velocity of about 1.5 km/s, wherein the porous skeleton remained nearly stationary and the burnout in the erosion region was small. Outside this zone, the phase velocities leveled off, followed by slow combustion according to law (4) at low pressure. Accordingly, noticeable acceleration of the wave did not occur. This situation is similar to the isothermal detonation described in [24, 25], including the value of the velocity wave  $D = \sqrt{(\gamma - 1)Q}$ .

Therefore, a combined mechanism of erosion with simultaneous fragmentation was considered. As in the previous case, for a given value of  $T_b$ , we selected the most suitable aerodynamic coefficient  $\theta$  for reproducing the kinematics. For  $T_b$  varying in the range  $(T_0 + 700)$ – $(T_0 + 1500)$  K, the coefficient  $\theta$  increases from 0 to 1.13. The kinematics was best reproduced for  $T_b = T_0 + 1200$  K: the curve of  $x(t)$  not only coincided with the experimental one at the beginning and end, but also passed near the experimental points throughout the calculation. The results for this variant are shown in Fig. 5.

Despite the satisfactory agreement of the kinematics, the density dynamics (see Fig. 5a) is very different from the experimental one (see Fig. 1a). As in previous variant, there is an initial density peak. Further, up to  $t = 5.5 \mu\text{s}$ , the calculated compaction is about 5 times less than the experiment value. Note that for other values of  $T_b$ , the kinematic agreement worsens without any improvement in the reproduction of the density dynamics. Thus, the erosive burning model does not describe the experiment. Note that this fact was found only due to the use of non-perturbing synchrotron diagnostics, which allows monitoring the internal structure of the charge.

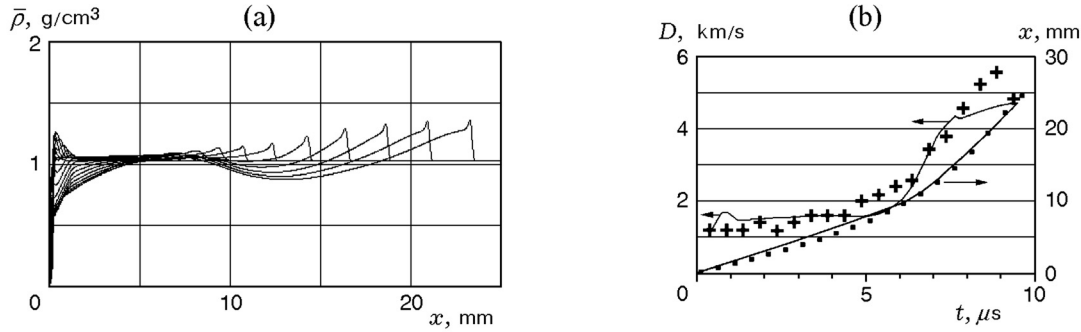


**Fig. 5.** Calculation of the regime shown in Fig. 1, taking into account erosion and aerodynamic fragmentation ( $T_b = T_0 + 1200$  K and  $\theta = 0.45$ ): (a) calculated density distribution along the charge axis (step  $0.5 \mu$ s); (b) kinematics of the wave front; points refer to the experimental data, and curves refer to the calculated results.

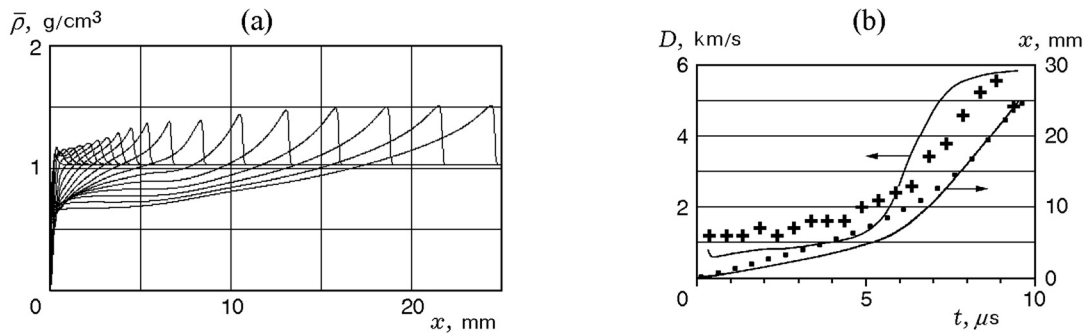


**Fig. 6.** Calculation of the regime shown in Fig. 1 taking into account ablation and aerodynamic fragmentation ( $T_b = T_0 + 10$  K,  $k = 1.4$ , and  $\theta = 0.45$ ): (a) calculated density distribution along the charge axis (step  $0.5 \mu$ s); (b) kinematics of the wave front; points are experimental data, and curves are calculated results.

### 3.3. Ablation and Fragmentation

Calculations have shown that the ablation mechanism and its combination with the standard combustion rate (4) do not lead to any reasonable results. As in the case of the erosive mechanism, high burning rate was localized in a thin layer at the wave front. Then the deceleration of the flow due to gas release and friction led to a decrease in the relative phase velocity and practical switching-off of the ablative mechanism. Slow combustion according to (4) in the main part of the charge could not sustain the acceleration of the wave.

In [8], a qualitative description of the experiment was obtained with simultaneous consideration of ablative burning and fragmentation by compaction. It is natural to expect that the inclusion of the aerodynamic fragmentation mechanism will improve the agreement with the experiment. Therefore, we performed a series of calculations with varying the ignition temperature  $T_b$  averaged over the solid phase, the ablation coefficient  $k$  in the burning rate law (15) and the aerodynamic coef-

ficient  $\theta$ . As in [8], the rates of burning by the ablative and standard mechanism were summarized for the same reasons as in (10). The results of calculation for the optimal variant are shown in Fig. 6.

Indeed, the agreement of the density profiles with the experimental were improved (see Fig. 6a and Fig. 8b [8]). In particular, the amplitudes of the profiles at the beginning of the process has increased significantly and approached the experimental ones. The density at the wave front increased monotonically except for the virtually unnoticeable initial peak. The kinematics is also better reproduced and can now be considered satisfactory. During the first  $5 \mu$ s, the wave velocity was about 30% lower than the experimental value.

Changing the model parameters compared to the above worsens the agreement of the density dynamics or kinematics. It is clear that this variant describes the experiment better than those shown in Figs. 4 and 5. It can be concluded that for a rough model such as that used, ideal agreement with the experiment could hardly be expected.

## CONCLUSIONS

The calculations have shown that each of the considered separate mechanisms of combustion intensification by itself does not describe the results of the experiment. From the possible combinations, the best agreement is provided by simultaneous consideration of ablation and fragmentation.

Note that the calculated density profiles were compared with experimental ones (see Fig. 1a) purely visually. A more detailed comparison would make sense if their similarity was higher, which was unattainable at modeling level used. At this stage, the resulting agreement can be considered acceptable.

Thus, the most plausible explanation for the rapid deflagration-to-detonation transition during high-enthalpy initiation is that the reaction is accelerated by the two processes: ablation (rapid combustion with dispersion of the evaporating layer on the particle surface due to shear instability) and particle fragmentation (in particular due to aerodynamic forces), which increases the specific surface.

We ought to note that the work in this direction was initiated by Professor Leonid Luk'yanchikov (died in 2013). These results clarify the nature of the process that Leonid Luk'yanchikov studied for more than 50 years.

The work was supported by the Russian Foundation for Basic Research (Grant No. 12-03-00077) and RAS Presidium Program No. 2 (Grant No. 7).

## REFERENCES

1. A. F. Belyaev, M. A. Sadovskii, and I. I. Tamm, "Application of the Similarity Law in Explosions to the Detonation Propagation Phenomenon," *Prikl. Mekh. Tekh. Fiz.*, No. 1, 3–17 (1960).
2. A. Ya. Apin, A. N. Afanasenkov, G. V. Dimza, and V. N. Stafeev, "On Detonation Transfer at a Distance," *Dokl. Akad. Nauk SSSR* **147** (5), 1141–1143 (1962).
3. L. A. Luk'yanchikov, "Initiation Systems Using Secondary Explosives," *Prikl. Mekh. Tekh. Fiz.* **41** (5), 48–61 (2000) [*J. Appl. Mech. Tech. Phys.* **41** (5), 806–817 (2000)].
4. A. F. Belyaev, V. K. Bobolev, I. A. Korotkov, A. A. Sulimov, and S. V. Chuiko, *Transition from Combustion to Explosion in Condensed Systems* (Nauka, Moscow, 1973) [in Russian].
5. G. E. Seay, L. B. Seely, "Initiation of a Low-Density PETN Pressing by a Plane Shock Wave," *J. Appl. Phys.* **32** (6), 1092–1097 (1961).
6. V. V. Andreev and L. A. Luk'yanchikov, "Mechanism of Propagation of Low-Velocity Detonation in Powdered PTEN on Spark Ignition," *Fiz. Goreniya Vzryva* **10** (6), 912–919 (1974).
7. V. V. Andreev, A. P. Ershov, and L. A. Luk'yanchikov, "Two-Phase Porous Low-Speed Detonation of a Porous Explosive," *Fiz. Goreniya Vzryva* **20** (3), 89–93 (1984) [*Combust., Expl., Shock Waves* **20** (3), 330–334 (1984)].
8. A. P. Ershov, A. O. Kashkarov, L. A. Luk'yanchikov, and E. P. Prueel, "Initiation of Detonation of a Porous High Explosive by a High-Enthalpy Gas Flow," *Fiz. Goreniya Vzryva* **49** (1), 91–105 (2013) [*Combust., Expl., Shock Waves* **49** (1), 79–91 (2013)].
9. A. P. Glazkova, *Catalysis of Combustion of Explosives* (Nauka, Moscow, 1976) [in Russian].
10. V. F. Kuropatenko, "Equation of State of Detonation Products of Compact Explosives," *Fiz. Goreniya Vzryva* **25** (6), 112–117 (1989) [*Combust., Expl., Shock Waves* **25** (6), 762–767 (1989)].
11. J. F. Baytos, B. G. Craig, A. W. Campbell, et al., *LASL Explosive Property Data* (University of California Press, Berkeley, CA, 1980).
12. W. H. Denton, "The Heat Transfer and Flow Resistance for Fluid Flow Through Randomly Packed Spheres," in *General Discussion on Heat Transfer* (Inst. of Mechanical Engineering and ASME, London, 1951), pp. 370–373.
13. V. M. Titov, Yu. I. Fadeenko, and N. S. Titova, "Acceleration of Solids by Shaped-Charge Explosion," *Dokl. Akad. Nauk SSSR* **180** (5), 1051–1052 (1968).
14. R. I. Nigmatulin, P. B. Vainshtein, and I. Sh. Akhatov, "Transition of Powdered Explosive Convective Combustion into Detonation," *Fiz. Goreniya Vzryva* **19** (5), 93–97 (1983) [*Combust., Expl., Shock Waves* **19** (5), 618–621 (1983)].
15. B. S. Ermolaev, B. V. Novozhilov, V. S. Posvyanskii, and A. A. Sulimov, "Results of Numerical Modeling of the Convective Burning of Particulate Explosive Systems in the Presence of Increasing Pressure," *Fiz. Goreniya Vzryva* **21** (5), 3–12 (1985) [*Combust., Expl., Shock Waves* **21** (5), 505–514 (1985)].
16. V. N. Vilyunov, "On the Theory of Erosive Burning of Gunpowder," *Dokl. Akad. Nauk SSSR* **136** (2), 381–383 (1961).
17. Ya. B. Zel'dovich, "On the Theory of Powder Combustion in Gas Flow," *Fiz. Goreniya Vzryva* **7** (4), 463–476 (1971).
18. V. K. Bulgakov and A. M. Lipanov, *Theory of Erosive Burning of Solid Propellants* (Nauka, Moscow, 2001) [in Russian].
19. S. S. Kutateladze and A. I. Leont'ev *Heat and Mass Transfer and Friction in a Turbulent Boundary Layer* (Energiya, Moscow, 1972) [in Russian].
20. H. Schlichting, *Boundary-Layer Theory* (McGraw Hill, New York, 1959).

21. E. P. Volchkov and V. P. Lebedev, *Heat and Mass Transfer in Near-Wall Flows* (Novosibirsk State Technical University, Novosibirsk, 2003) [in Russian].
22. J. M. Lenoir, G. Robillard, "A Mathematical Method to Predict the Effects of Erosive Burning in Solid-Propellant Rockets," in *Proc. 6th Symp (Int.) on Combustion, New Haven, CO, 1956* (Reinhold, New York, 1956), pp. 663–667.
23. A. G. Merzhanov and A. E. Averson, "The Present State of the Thermal Ignition Theory: An Invited Review," *Combust. Flame* **16** (1), 89–124 (1971).
24. A. P. Ershov, "Isothermal Detonation and its Stochastic Modeling," *Fiz. Goreniya Vzryva* **30** (3), 112–124 (1994) [*Combust., Expl., Shock Waves* **30** (3), 366–376 (1994)].
25. A. P. Ershov, "Isothermal Detonation," *Combust. Flame* **101** (3), 339–346 (1995).